Molecular Dynamics Numerical and Experimental Analysis of Fretting Wear Mechanism of Variable Gauge Bogie

Jiaxin Ji (jijiaxin0226@163.com)
China University of Petroleum Huadong - Qingdao Campus https://orcid.org/0000-0002-1349-6864
He Sheng
China University of Petroleum Huadong - Qingdao Campus
Reng Yanping
Southwest Jiaotong University

Research Article

Keywords: Molecular Dynamics, Fretting Wear, Variable Gauge Bogie, MoS2 Coating, Ion Nitriding

Posted Date: March 17th, 2022

DOI: https://doi.org/10.21203/rs.3.rs-1348199/v1

Abstract

Under the "One belt, One road" strategy, the trade in goods is more frequent in diverse countries. The difference in train gauge between countries often leads to low efficiency of freight transportation. In several schemes, the variable gauge bogie can efficiently solve this problem. The fretting wear between the axles and wheels of train gauge changeable bogies may cause the connection relaxation and failure in the actual working process, resulting in potential safety hazards. Diverse experimental researches show that surface treatment technology can effectively reduce the friction and wear between axles and wheels. However, its micro wear reduction mechanism is not clear, to date. Therefore, the three-dimensional fretting wear model of bogie axle and wheel is established by molecular dynamics method in this paper. The wear reduction mechanism of surface treatment technology is then clarified from the micro point of view, and also verified by experiments. The results show that there is micro convex contact between the two surfaces under the contact stress. The micro convex is extruded and deformed, hence forming an adhesion. Whereas, the convex adhesion is desorbed by the shear force during separation, resulting in fretting wear. Since the wear reduction is caused by the reduction of transverse force, good lubrication and wear reduction effect can be achieved by MoS_2 coating and nitriding. The surface treatment of MoS_2 coating also reduces the friction coefficient between axles and wheels along with improving load bearing. Whereas, the friction coefficient can be decreased by increasing the nitriding amount.

1 Introduction

With the vigorous development of the global trade integration, transnational cargo transportation is becoming ever more frequent. The railway’s development has turned into a crucial goal of various countries due to its low cost and huge transportation capacity [1, 2]. However, due to the differences in train gauges in various countries, it takes a lot of time to replace any identical device during the transportation, which leads to a great inconvenience of transnational cargo transportation under the strategy of "One Belt and One Road" [3]. Variable gauge bogie wheelsets can realize migration on different gauge tracks, and have the advantages of low cost and high efficiency [4, 5]. Meanwhile, the axle and wheel mating mode make it easy to produce axial slip, impact and vibration between the axles and wheels, resulting in wear of key components [6]. Since the available research on wear mechanism is not very comprehensive [7–13], the present study of fretting wear is focused on macroscopic experiment.

The proposal of the "Hard Ball" model and the successful development of multi-body Embedded-Atom Method (EAM) [14–16] ake molecular dynamics become a significant method to study the properties of metal materials at the nanoscale level [17]. Various researchers analyzed the fretting on the surface of metal Zr and alloy AZ91, while others have studied the tribological properties of coated materials such as MoS_2 based on molecular dynamics method [18–23]. Their results show that the surface treatment can reduce wear by changing the fretting area. However, in the present microscopic fretting wear mechanism analysis, the research focus is mainly on the single-atom metal or simple metal compounds. Furthermore, the molecular dynamics analysis of complex alloy structure is rarely seen [24].

To solve the above-mentioned problems, a variable gauge bogie model with complex alloy structure has been established by molecular dynamics method in this paper. The microscopic wear mechanism and wear reduction mechanism of surface treatment of bogie have also been revealed by combining the simulation and experiment. The results are highly significant for the wear resistance design of variable gauge bogie and the microcosmic modeling of complex alloy.

2 Configuration Of The Exoskeleton Arm

Previous researches [25, 26] demonstrate that DZ2 steel of axle material and D2 steel of wheel material belong to face-centered cubic lattice (FCC), and their lattice constants are a = b = c = 3.43 mm and α = β = γ = 90°. Therefore, Fe matrix is extended based on the face-centered lattice under this parameter. Fe atoms have been randomly replaced in the matrix according to the material composition in Table 1 to complete the doping in DZ2 and D2 steel alloys. The final molecular dynamics model is shown in Fig. 1.

Table 1
Material compositions

Material	DZ2	D2
C	0.24 ~ 0.32	0.48 ~ 0.58
Si	0.20 ~ 0.40	0.65 ~ 0.80
Mn	0.60 ~ 0.90	≤ 0.015
P	≤ 0.01	≤ 0.015
S	≤ 0.01	≤ 0.030
Cr	0.90 ~ 1.20	≤ 0.08
Mo	0.20 ~ 0.30	≤ 0.030
Ni	0.50 ~ 1.50	≤ 0.016

The whole model is divided into three parts: fixed layer, thermostat and free layer, as demonstrated in Fig. 1. In the present model, the boundary layer fixed model does not move in the y direction. Therefore, the y direction is an aperiodic boundary, and the x and z directions are periodic boundaries. The thermostat is used to adjust the ambient temperature of the system, whereas the initial temperature is set at 300 K. The free layer moves in accordance with Newton's law of motion, and the data needed for the micro-friction of wheel and axle are then obtained. A rough peak with height of 20.58 Å was established in the free layer to simulate the fretting wear process. The micro-canonical ensemble, also known as NVE ensemble, is selected for the simulation of the working condition between the wheel and axle. This way, the whole system has no energy and particle exchange with the outside world.

EAM is suitable for intermetallic molecular dynamics simulation [27]. In this paper, EAM is used for relaxation processing to accurately characterize the interactions between atoms in the alloy under stable

state. The EAM potential function is shown in Eq. (1) [14]:

$$E = \frac{1}{2}\sum_{i=1}^{N}\sum_{j=1\neq i}\varphi_{ij}(r_{ij}) + \sum_{i=1}^{N}F_i(\rho_i)$$

1

Where E represents the sum of potential energy between atoms, φ_{ij} represents the pair potential of interatomic interaction, r_{ij} represents the distance between atoms, F_i is the energy required when atom i is embedded into the position of electron density unit 1, and ρ_i shows the local electron density generated by all atoms in the system at the position of atom i.

Lennard-Jones (LJ) potential consists of a simple structure with high calculation efficiency. It can simultaneously calculate the interaction force between the two interfaces with high calculation efficiency[28]. Hence, LJ potential has been used in this paper to represent the interaction force between wheel and axle. The potential function form of LJ method is shown in Eq. (2) [28]:

$$U_{LJ}(r) = 4\varepsilon[(\frac{\sigma}{r})^{12} - (\frac{\sigma}{r})^{6}]$$

2

where, U_{LJ} represents the sum of potential energy between atoms, ε is the potential well depth that reflects the strength of the interaction between two atoms, σ is the fixed distance between atoms when the interaction potential is equal to zero, and r is the distance between two atoms at any instance.

According to the addition and subtraction properties of Eq. (2) regarding r, an increase in r to a certain value leads the potential energy of LJ to zero. The distance at this point is known as truncation radius r_c. This phenomenon occurs when the distance between the analyzed atom and the observed atom is greater than r_c. Due to the relatively greater spacing between atoms as compared to the truncation radius, the interaction force becomes insignificant [29]. Hence, the force between the two atoms is not calculated. The truncation radius r_c is calculated to be 11 Å, according to the atomic parameters of wheel and axle material [29].

3 Fretting Wear Numerical Results And Analysis

The research has been conducted using Large-scale Atomic/Molecular Massively Parallel Simulator (LAMMPS) for calculating and using Visual Merchandising (VMD) for post-processing. The timestep and the output interval τ is set as 0.0025 fs and 1.25 fs, respectively. The wheel DZ2 steel is fixed, and the axle DZ2 steel moves horizontally at a constant speed of 2.5 m/s. Figure 2 demonstrates the fretting wear phenomenon between wheels and axles. The two rough peaks completely contact and overlap at 8τ (Fig. 2(a)). Whereas, the two rough peaks are separated at 15τ (Fig. 2(b)). The two rough peaks contact for the second time at 45τ (Fig. 2(c)). The residual heights of the two rough peaks are about 17.15 Å, and The system begins to stabilize at 200τ.

Figure 3 depicts a detailed representation of the deformation of the rough peak during the fretting wear. The contact of the two rough peaks resulted in obvious extrusion deformation, as shown in Fig. 3(a). This lead to an interatomic adhesion (Fig. 3(b)), causing some atoms to be desorbed under the shear force (Fig. 3(c), top view). Therefore, the general process of fretting wear can be deduced as following steps:

1. The contact stress makes the micro-bumps contact, resulting into extrusion deformation and adhesion.

2. During the separation, the protruding adhesive is desorbed by the shear force that leads to the fretting wear.

Figure 4 shows the varying regulation of friction coefficient with time in fretting friction process. It can be visualized that the friction coefficient surges during the contact extrusion deformation and reaches a peak value at the maximum contact, which is the maximum extrusion deformation. Due to the influence of atomic bond formation and contact point growth, the peak friction coefficient is found to be greater than one [26]. After that, the shear force results in the breaking of the atomic bond, and atoms are desorbed from the matrix. Meanwhile, the friction coefficient keeps on decreasing, simultaneously. The subsequent cyclic friction did not form a large extrusion deformation as with the first contact. Hence, the friction coefficient oscillated at a smaller value with an average single-peak friction coefficient of 0.225.

4 Fretting Wear Reduction Mechanism Of Surface Treatment Technology And Experimental Analysis

The damage and failure of materials mostly begin with the surface damage, for which there is a modeling lubrication surface treatment technology for materials [30]. In the surface treatment process, nitriding and coating MoS_2 can achieve good anti fretting wear effect. Therefore, this chapter explores its wear reduction mechanism [31].

4.1 Fretting Wear reduction mechanism and experimental analysis of MoS_2 model

Various researches have demonstrated that the solid lubrication coating of MoS_2 bonded on LZ50 steel has good resistance to radial fretting wear [6–9]. Therefore, the surface MoS_2 coating was added on the basis of the model to analyze the influence of surface treatment technology on fretting wear, as presented in Fig. 5.

The revised model is depicted in Fig. 5 (a), and the simulation results obtained are shown in Fig. 5 (c). It can be seen that the surface treated by MoS_2 produces fretting wear behaviors, such as extrusion deformation, adhesion and desorption fretting. The varying regulation of friction coefficient with time (Fig. 5 (b)) shows that the average friction coefficient is 0.218, which is lower than the corresponding friction coefficient of the untreated model. The results exhibit that the coating MoS_2 can significantly reduce the wear, and protect the metal from fretting friction.

To further optimize the ideal conditions of MoS_2 coating, simulation analysis method was applied to observe the number of coating layers, temperature and load, and the obtained varying regulation of friction coefficient with time, as shown in Fig. 6. It has been observed that the friction coefficient has no obvious change trend with the coating thickness and temperature changing (Fig. 6(a) and 6(b)). Whereas, the friction coefficient values have been found to decrease with the increase of load (Fig. 6(c)). This shows that the friction coefficient of MoS_2 is inversely correlated with the load. Several researchers have conducted in-depth studies on MoS_2 lubrication characteristics, and found that the friction coefficient decreases with the increase of load [32–34]. The simulation results are in line with those published above. Therefore, it is concluded that MoS_2 coating can play a crucial wear reduction lubrication effect at both high and low temperatures. However, the wear reduction effect is mainly influenced by the load, and the lubrication effect and the pressure are in direct relation with each other.

The surface of DZ2 steel was coated with MoS_2 with bonding solid lubricant layer. The workpiece obtained by this method has been found to have good fretting wear resistance [35]. WTM-2E friction and wear tester machine is specially used to test the friction coefficient and wear resistance of various coatings or solid lubricating materials, with an advantage of high testing accuracy and simple operational process. Hence, the friction coefficient of the workpiece coated with MoS_2 was measured by WTM-2E under diverse loading. In the experiments, the speed was set as 400 rpm, a loading radius of 3 mm and a cylindrical fixture with a probe diameter of 2.4 mm was used for testing. Three groups of friction and wear experiments were carried out under different pressures of 0.043 MPa (20 grams), 0.108 MPa (50 grams) and 0.152 MPa (70 grams). The average and maximum friction coefficients obtained are presented in Table 2. The average friction coefficient of each group is approximately 0.1, which is lower than that of the untreated workpiece (0.225). The decline rate was 55.6%, as shown in Fig. 4. This indicates that the surface coating MoS_2 significantly reduces the wear. Furthermore, the average friction coefficient gradually decreases with the increase of load, which is also in line with the numerical findings.

Table 2
Material compositions

Load	0.043 MPa	0.108 MPa	0.152 MPa
f_{avg}	0.111	0.103	0.990
f_{max}	0.172	0.184	0.264

4.2 Fretting Wear reduction mechanism and experimental analysis of nitriding model

The surface chemical composition and organization considerably alter after the nitriding treatment of the workpiece. As shown in Fig. 7 (a), Nitrogen atoms were swapped, randomly, and potential functions were reasonably chosen to characterize the nitriding model after relaxation [36]. The varying regulation of

friction coefficient with time after simulation has been shown in Fig. 7 (b). Statistically, the maximum friction coefficient of the nitriding model is 6.83, and the average friction coefficient is 0.194. Compared with the prior untreated model group, the friction coefficient of the two groups is decreased, indicating that the nitriding treatment can greatly reduce fretting wear. This can be attributed to the formation of high hardness value of nitride Fe_4N between nitrogen and metal after nitriding. Hence, the nitriding treatment also enhances the hardness and wear resistance of the steel surface.

Varying the nature of nitriding process will lead to the modification of compound and nitrogen content in bogie, thus affecting the lubrication effect [37]. Figure 8 compares the influence of different nitriding depth, nitriding amount and load on the nitriding model's wear reduction effect. It can be seen that the friction coefficient does not significantly alter with the depth and load of nitriding treatment. However, the friction coefficient decreases with the increase of the nitriding amount. The results depict that a fine wear reduction effect can be attained by increasing the nitriding amount. However, the increase of nitriding amount in the alloy will also lead to low plasticity and toughness of the wheel [38]. Therefore, relevant factors need to be comprehensively addressed to choose the optimized amount of nitriding for the industrial application of the process.

The ion nitriding workpiece can be generated by the application of three-stage nitriding method with the best anti-fretting wear effect [39]. Therefore, to verify the accuracy of the simulation analysis, the current study adopts the three-stage nitriding method to treat the workpiece surface. WTM-2E was used to carry out the experimental study under the pressure values of 0.043 MPa, 0.108 MPa and 0.152 MPa, respectively. The remaining experimental conditions are consistent with the ones described in the section 4.1. All other parameters were consistent with the experimental setup of coated MoS_2. The average and maximum friction coefficients obtained under different loads are presented in Table 3. Experimental data show that the value of friction coefficient of nitriding workpiece is less than that of the untreated workpiece under various load conditions. This indicates that the nitriding treatment method is far effective in reducing the wear. Furthermore, it can be observed that the average friction coefficient of nitriding workpiece is not influenced by the variation of load, when the analysis of the average friction coefficient has been performed under each load.

Table 3
The friction coefficient of nitriding workpiece under different loads

Load	0.043 MPa	0.108 MPa	0.152 MPa
f_{avg}	0.206	0.215	0.208
f_{max}	0.274	0.275	0.291

4.3 Fretting wear reduction mechanism analysis

The wear reduction mechanism of the surface treatment process was studied by the untreated models, i.e. nitriding model (20%) and MoS_2 model (100 Kcal/mole.Å). The varying regulation of positive pressure

(Y direction) and friction (X direction) of the three output models in fretting wear are shown in Fig. 9 It can be visualised that the positive pressure of all models has a similar trend over time (Fig. 9 (a)). The oscillation becomes obvious when the contact and the detachment occur, and the oscillation starts to weaken after the contact. The friction coefficient of MoS_2 model is found to be the lowest followed by the nitriding model, and the untreated model is the largest, as shown in Fig. 9 (b). The discussed results are consistent with the simulation results of friction coefficient. Therefore, by comprehensive analysis of the discussed results, it can be concluded that the decrease of friction coefficient after surface treatment is not due to the change of positive pressure, but mainly due to the decrease of transverse friction force (bond-breaking shear force) during the desorption fracture.

5 Conclusion

Aiming at the fretting wear behavior, the fretting wear model between bogie wheel and axle was established from the microscopic point of view by using molecular dynamics method. The fretting wear phenomenon and the changing regulation of friction coefficient with time were analyzed. The results demonstrate that the general process of fretting wear can be presented as follows:

1. The micro-bumps contact under stress, then the micro-bumps extrude and form adhesion.

2. The adhesion is desorbed by the shear force during the separation to form fretting wear.
On the basis of fretting wear model, two molecular dynamics models of coated MoS_2 and ion nitriding surface treatment were established, respectively. Simulation and experimental results conclude that the surface treatment technology can play a vital role in effectively reducing the wear effect. It is found that the friction coefficient of coated MoS_2 model significantly decreases by increasing the load. Whereas, a considerable decrease of the friction coeffocoent of nitriding model has been observed with the increase of nitriding amount. By analyzing the varying regulation of transverse and longitudinal force with time, it is found that the reduction of transverse force is the principal reason for reducing the wear of surface treatment applications.

Declarations

Acknowledgements

The authors sincerely thanks to Professor Cai Zhenbing of Southwest Jiaotong University for his critical discussion and reading during manuscript preparation.

Funding

This research was funded by the National Natural Science Foundation of China (NSFC) (51805547), the Shandong Provincial Natural Science Foundation (ZR2017LEE016), and Fundamental Research Funds of Central Universities (18CX02018A).

Availability of data and materials

The datasets supporting the conclusions of this article are included within the article.

Authors' contributions

The author' contributions are as follows: Ji Jiaxin was in charge of the whole trial; He Sheng wrote the manuscript; Ren Yanping assisted with sampling and laboratory analyses.

Competing interests

The authors declare that they have no known competing financial interests or personal relationships that could have appeared to influence the work reported in this paper.

References

1. Liu W. (2015). Scientific understanding of the Belt and Road Initiative of China and related research themes. Progress in Geography, 34(5). doi:10.11820/dlkxjz.2015.05.001.
2. Wang C, Lim M K, X Zhang, et al. (2020). Railway and road infrastructure in the Belt and Road Initiative countries: Estimating the impact of transport infrastructure on economic growth. Transportation Research Part A: Policy and Practice, 134:288–307. doi: 10.1016/j.tra.2020.02.009.
3. Mu-Yao Li, Fu Li, Huang Y H, et al. (2017). Development and present situation of gauge-changeable bogie. Electric Locomotives & Mass Transit Vehicles. doi: 10.16212/j.cnki.1672-1187.2017.05.001.
4. Shi H, Guo J, Wang Y. (2020). Dynamic Performance of High-speed Gauge-changeable Railway Vehicle. Journal of Mechanical Engineering 56(20):98. doi: 10.3901/JME.2020.20.098.
5. Zhou P Y, Wu P B. (2012). Study on Fatigue Strength for Axle of High Speed EMU. Advanced Materials Research, 479–481:965–970. doi: 0.4028/www.scientific.net/AMR.479-481.965.
6. Zxa B, Jpa C, Jl A, et al. (2019). Study on fretting wear and tribo-chemical behavior of LZ50 axle steel in torsional fretting fatigue. Wear, 426–427:704–711. doi: 10.1016/j.wear.2018.12.074.
7. Luo J, Zhu M H, Wang Y D, et al. (2011). Study on rotational fretting wear of bonded MoS_2 solid lubricant coating prepared on medium carbon steel. Tribology International, 44(11). doi: 10.1016/j.triboint.2010.10.011.
8. Li Z Y, Cai Z B, Cui X J, et al. (2021). Influence of nanoparticle additions on structure and fretting corrosion behavior of micro-arc oxidation coatings on zirconium alloy. Surface and Coatings Technology, 410: 126949. doi: 10.1016/j.surfcoat.2021.126949.
9. Cai Z B, Zhu M H, Zheng J F, et al. (2009). Torsional fretting behaviors of LZ50 steel in air and nitrogen. Tribology International, 42(11–12):1676–1683. doi: 10.1016/j.triboint.2009.04.031.
10. He-Gen G U, Cai Z B, Yue W, et al. (2013). Torsional Fretting Wear of Sulfurized-nitrided Layers Prepared on Axle Steel. Journal of Materials Engineering, 3(7):66–72(7). doi: 10.3969/j.issn.1001-4381.2013.07.013.

11. Li X, Ren Z, Xu N. (2018). Dynamic Performance Analysis of High-speed Vehicle Based on Optimization of Bogie Suspension Parameters and Tread Conicity. Tiedao Xuebao/Journal of the China Railway Society, 40(3):39–44. doi: 10.3969/j.issn.1001-8360.2018.03.006.
12. Qin Q B, Shengchuan W U, Nan H Y, et al. (2019). Fatigue strength and residual life assessment of high-speed railway vehicle used S38C hollow axles. Scientia Sinica Technologica, doi: 10.1360/SST-2019-0040.
13. Alder B J, Wainwright T E. (1957). Phase Transition for a Hard Sphere System. Journal of Chemical Physics, 27(5):1208–1209. doi: 10.1063/1.1743957.
14. Daw M S, Baskes M I. (1984). Embedded-atom method: Derivation and application to impurities, surfaces, and other defects in metals. Physical Review B Condensed Matter, 29(12):6443–6453. doi: 10.1103/PhysRevB.29.6443.
15. Springborg M. (2012). *Theoretical Studies of Structural and Electronic Properties of Clusters*. Springer Netherlands.
16. Guo Shaowen, Li Libo, Zhang Guangyu, et al. (2008). Adhesion analysis of electroless Ni coating on SiCp/Al composite mirror substrate. Rare Metal Mater Eng, 37 (6):960. doi: 10.1016/S1875-5372(09)60029-1.
17. Srivastava Isha, Kotia Ankit, Ghosh Subrata Kumar, et al. (2021). Recent advances of molecular dynamics simulations in nanotribology. Journal of Molecular Liquids, 335. doi: 10.1016/j.molliq.2021.116154.
18. Bin Shen, Fanghong Sun. (2008). Molecular dynamics investigations on the atomic-scale frictional behavior of diamond films. J Comput Theoretical Nanosci, 8 (5):1556
19. Pan S, Yin N, Zhang Z. Molecular Dynamics Simulation for Continuous Dry Friction on Fretting Interfaces. Journal of Mechanical Engineering, 2018. doi: 10.1166/jctn.2008.823.
20. Zhu Kehao, Zhang Xiaoyu, Yuan Xinlu, et al. (2021). Molecular dynamics simulation of grain size effect on friction and wear of nanocrystalline zirconium. *Proceedings of the Institution of Mechanical Engineers*, 235(6). doi: 10.1177/1350650120945079.
21. Deepak Kumar, Saurav Goel, Nitya Nand Gosvami, et al. (2020). Towards an improved understanding of plasticity, friction and wear mechanisms in precipitate containing AZ91 Mg alloy. *Materialia*, 10. doi: 10.1016/j.mtla.2020.100640.
22. Peter Serles, Hao Sun, Guillaume Colas, et al. (2020). Structure-Dependent Wear and Shear Mechanics of Nanostructured MoS_2 Coatings. Advanced Materials Interfaces, 7(14). doi: 10.1002/admi.201901870.
23. Serles P, Gaber K, Pajovic S, et al. (2020). High Temperature Microtribological Studies of MoS_2 Lubrication for Low Earth Orbit. *Lubricants*. doi: 10.3390/lubricants8040049.
24. Ming-Yu Hu, Jie Yu, Xiao-Long Zhou, et al. (2019). Surface layer structure change and tribological property of Cu/FeS composite under electric field. *Rare Metals*, 38(9). doi: CNKI: SUN: XYJS.0.2019-09-011.

25. Zhang D. (1998). Structure and Property of Cr12Mo1V1 Steel. *Heat treatment of metals*. doi: CNKI: SUN: JSRC.0.1998-04-000.
26. Uehara T & Tamai T. (2005). Molecular dynamics simulation on shape-memory effect in Ni-Al alloy by using EAM potential. Transactions of the Japan Society of Mechanical Engineers, 71(705), 717–723. doi: 10.1299/kikaia.71.717
27. Liu G W. (2008). Forging process of punching and hole-expanding for Cr12Mo1V1 tool steel. Forging & Stamping Technology. doi: 10.3969/j.issn.1000-3940.2008.01.004.
28. Deng P, Ovcharenko A, Tangaraj R, et al. (2014). Investigation of lubricant transfer between slider and disk using molecular dynamics simulation. Tribology Letters, 53(1), 373–381. doi: 10.1007/s11249-013-0277-9.
29. Verlet L. (1967). Computer "experiments" on classical fluids. I. thermodynamical properties of Lennard-Jones molecules. Physical Review, 159(1), 98–103. doi: 10.1103/PhysRev.159.98.
30. Xuejie Sun. (2011). *A Study on Tribology Behaviors of Nitrided and Sulfur-nitrided Surfaces under Oil Lubrications*. (Doctoral dissertation, China University of Geosciences, Beijing).
31. Wen Yue, Xuejie Sun, Wang Chengbiao, et al. (2011). A comparative study on the tribological behaviors of nitrided and sulfur-nitrided 35CrMo steel lubricated in pao base oil with modtc additive. Tribology International. doi:10.1016/j.triboint.2011.08.017.
32. Clauss F J. (1972). Solid lubricants and self-lubricating solids. *New York Academic Press*, -1(-1), 164–194.
33. Fusaro R L. (1978). A comparison of the lubricating mechanisms of graphite fluoride and molybdenum disulfide films. *Intern. Conf. on Solid Lubrication*.
34. Luo J. (2012). Rotational Fretting Wear Characteristics of Bonded Molybdenum Disulfide Solid Lubrication Coating. Journal of Mechanical Engineering, 48(17):100. doi: 10.3901/JME.2012.17.100.
35. Zhu M H & Zhou Z R. (2001). An investigation of molybdenum disulfide bonded solid lubricant coatings in fretting conditions. Surface & Coatings Technology, 141(2–3), 240–245. doi: 10.1016/S0257-8972(01)01194-X.
36. Menthe E, Rie K T. (1999). Further investigation of the structure and properties of austenitic stainless steel after plasma nitriding. Surface and Coatings Technology, 116(none):199–204. doi: 10.1016/S0257-8972(99)00085-7.
37. Li S, Zhang G, Wang H, et al. (2012). Effect of different tempering on plasma nitriding of 42CrMo steel. Jinshu Rechuli/Heat Treatment of Metals, 37(12):92–94. doi: 10.13251/j.issn.0254-6051.2012.12.016.
38. Yin G Q, Huang Z Y, Yang C F, et al. (2008). Effects of nitrogen content and tmcp on microstructure and mechanical properties of v-n micro-alloying steels. Heat Treatment of Metals. doi: CNKI: SUN: JSRC.0.2008-03-001.
39. Long F J, Zhou Y, Kang G Y, et al. (2007). Review of recently developed plasma nitriding technologies. Metal Hotworking Technology. doi: 10.3969/j.issn.1001-3814.2007.06.022

Figures

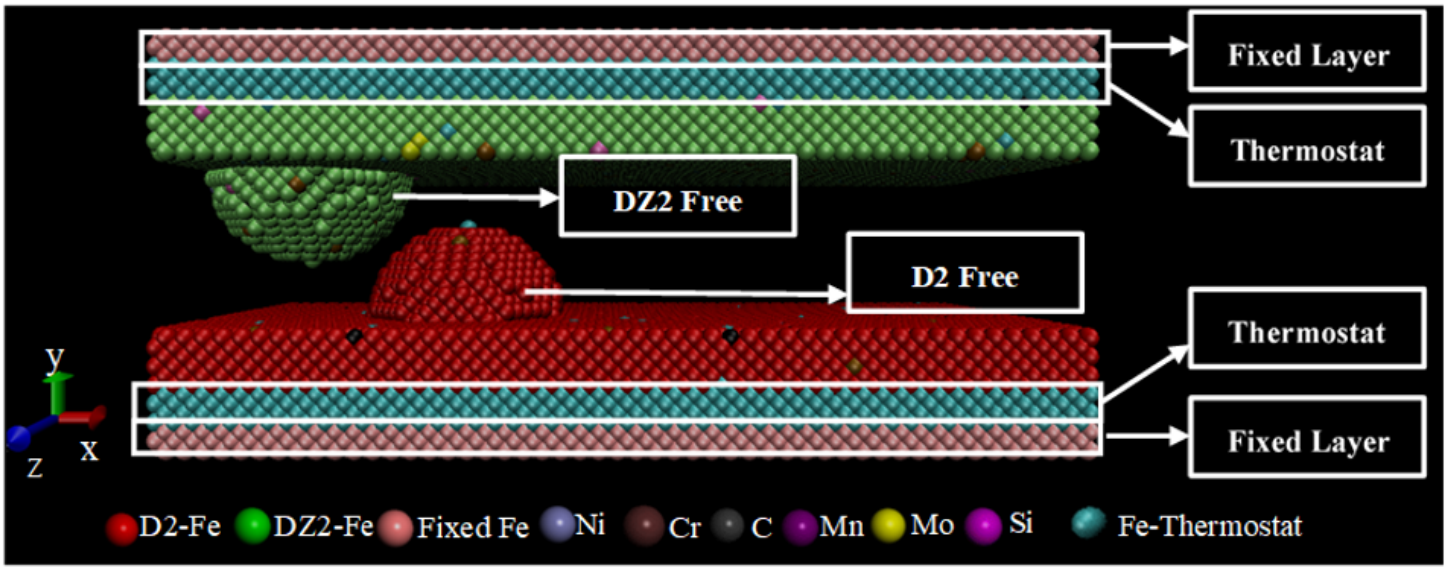

Figure 1

Molecular dynamics simulation model between wheels and axles

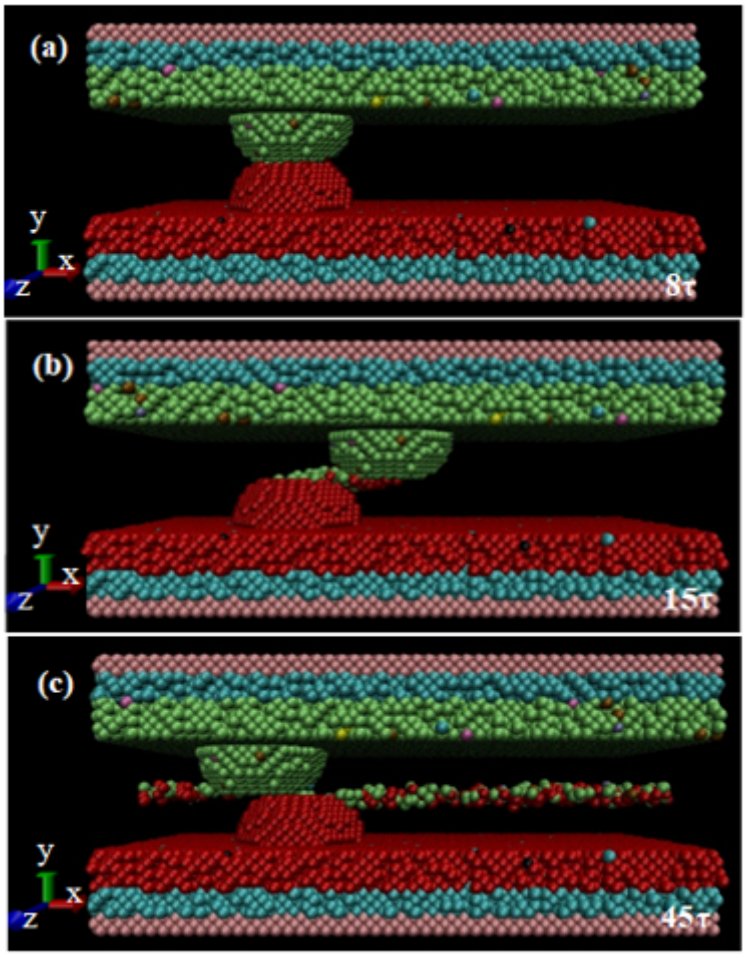

Figure 2

Fretting friction-wear process for single rough peak. (a) For 8τ Wear during operation; (b) For 15τ Wear during operation; (c) 45τ Wear during operation.

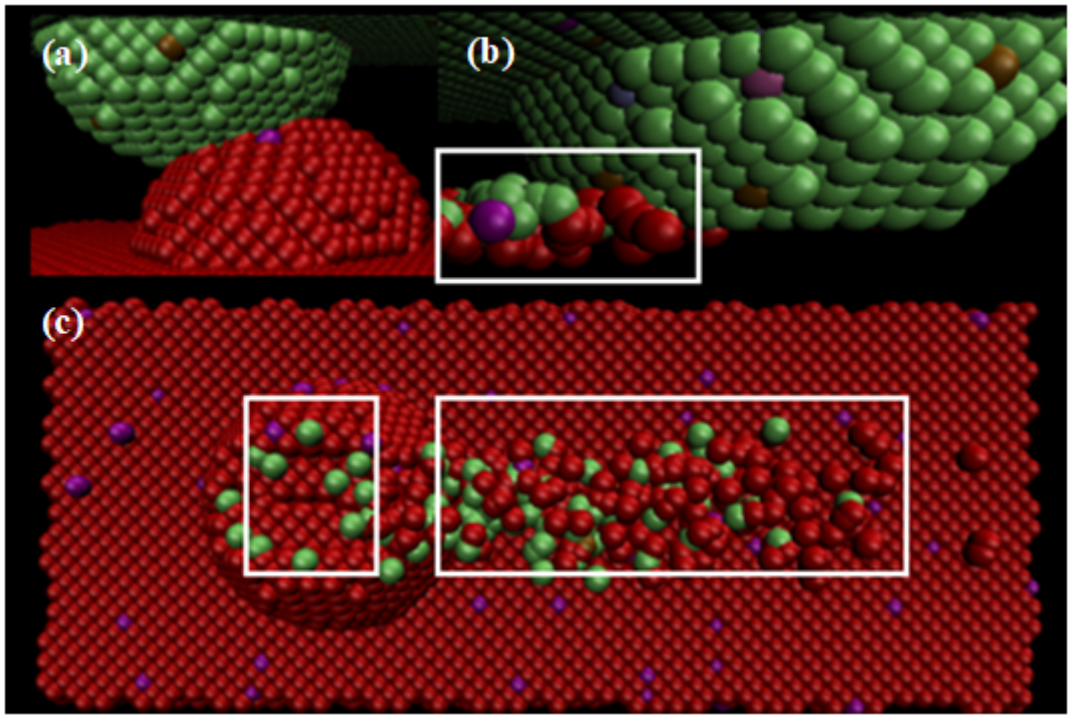

Figure 3

Characteristics of fretting friction behavior: (a) extrusion, (b) adhesion, (c) desorption.

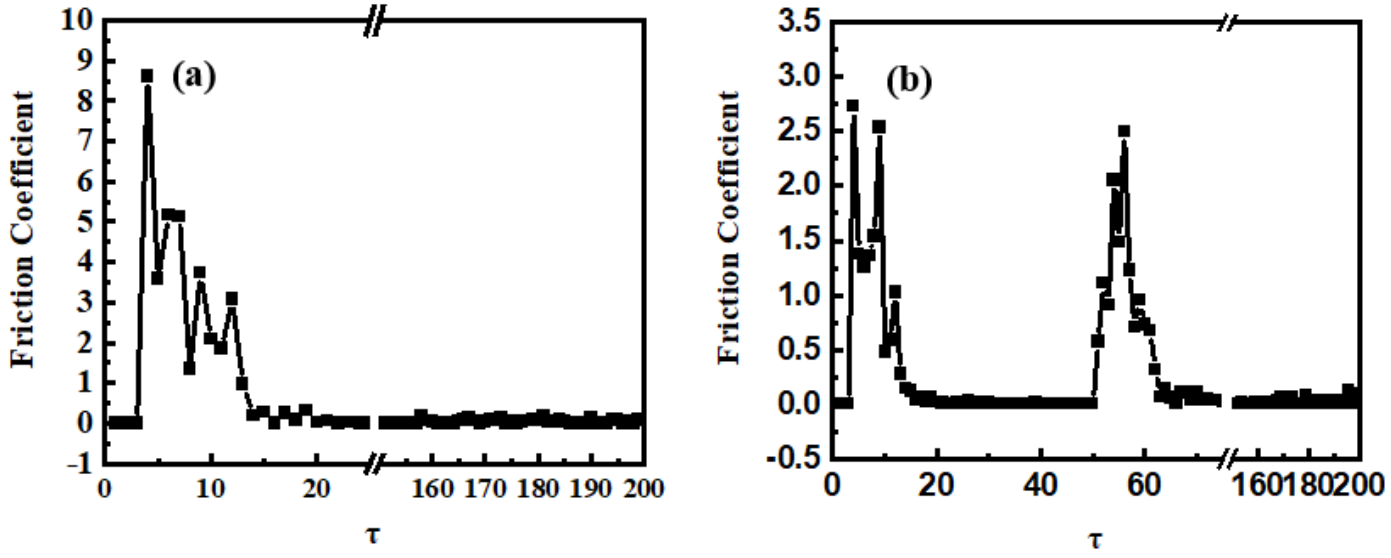

Figure 4

(a) Single. (b) Double rough peak's changing regulation of friction coefficient.

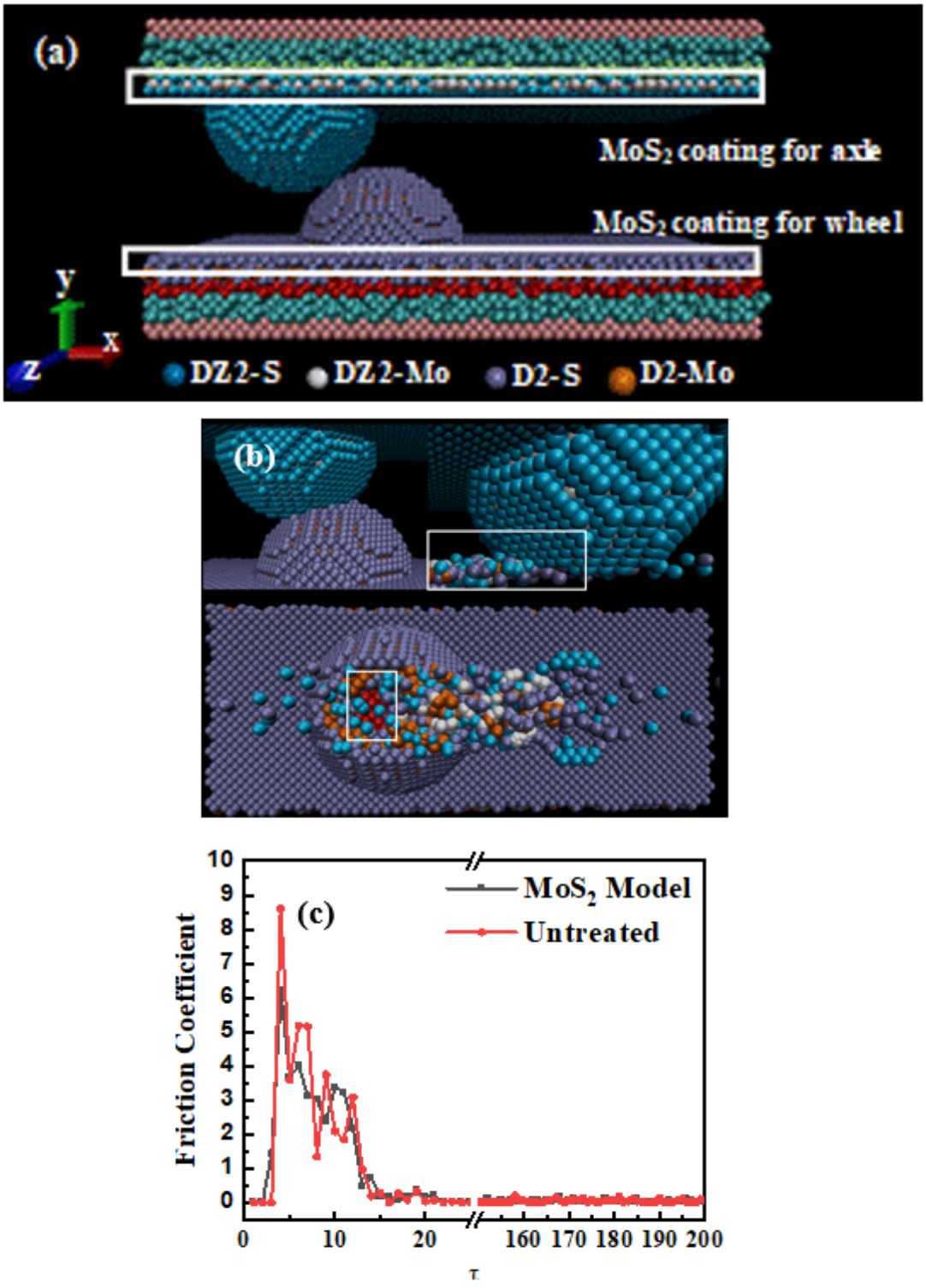

Figure 5

(a) Molecular dynamics simulation model of MoS_2 surface coating, (b) Characteristics of fretting friction behavior of MoS_2 model, (c) Changing regulation of friction coefficient of coated MoS_2 model.

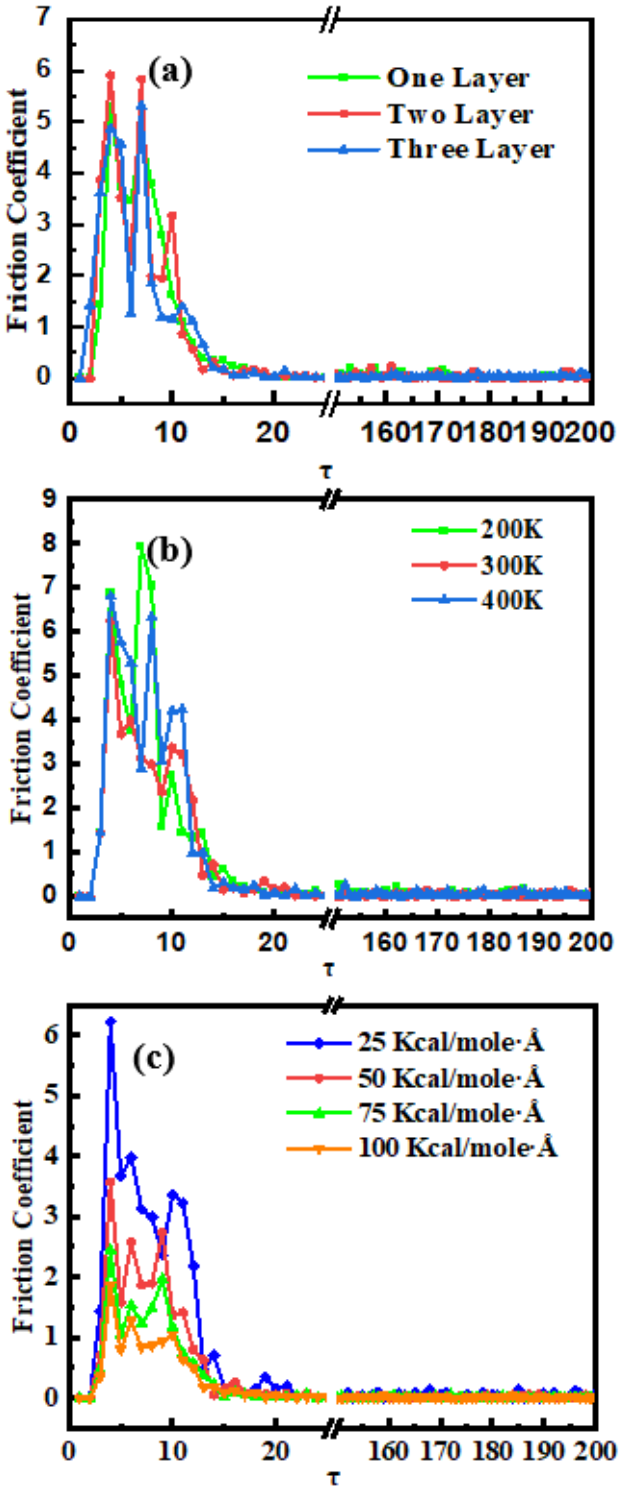

Figure 6

Varying regulation of friction coefficient with (a) number of coating layer variation, (b) temperature variation and (c) load fluctuation

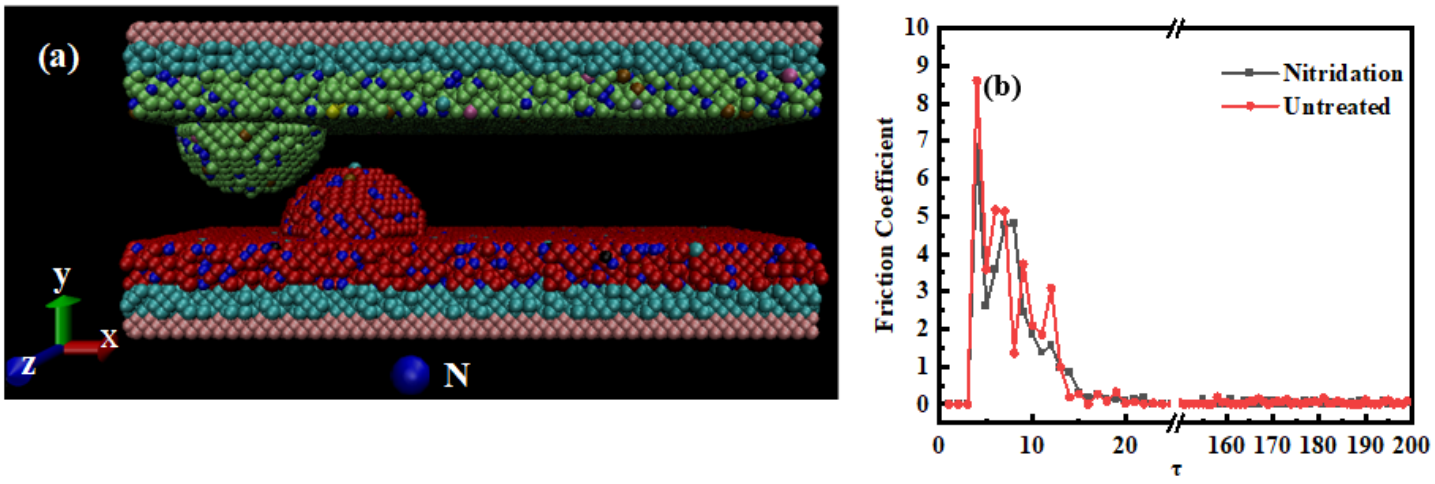

Figure 7

(a) Molecular dynamics simulation model of nitriding model, (b) Changing regulation of friction coefficient of nitriding model and untreated model.

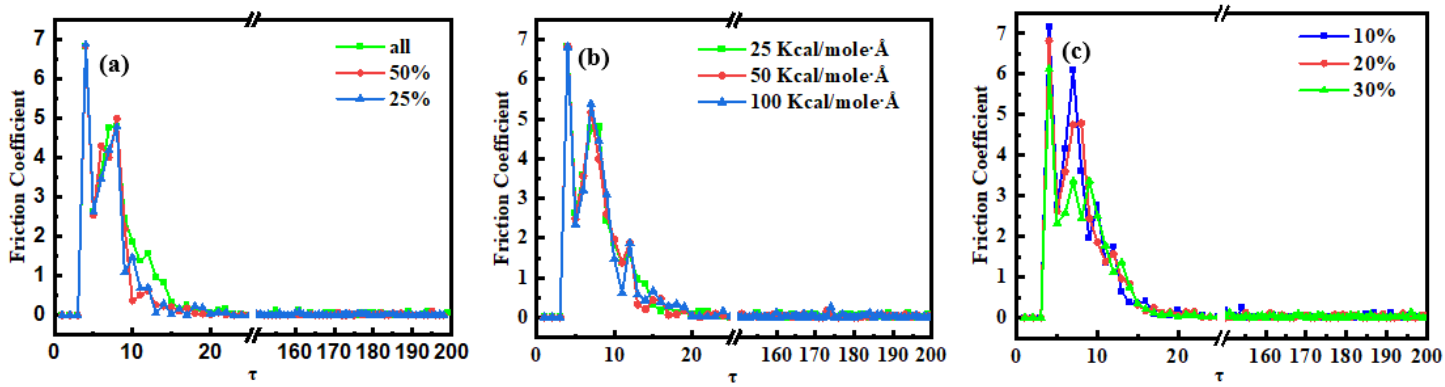

Figure 8

Changing regulation of friction coefficient with (a) nitriding depth variation, (b) load fluctuation and (c) nitriding quantity variation.

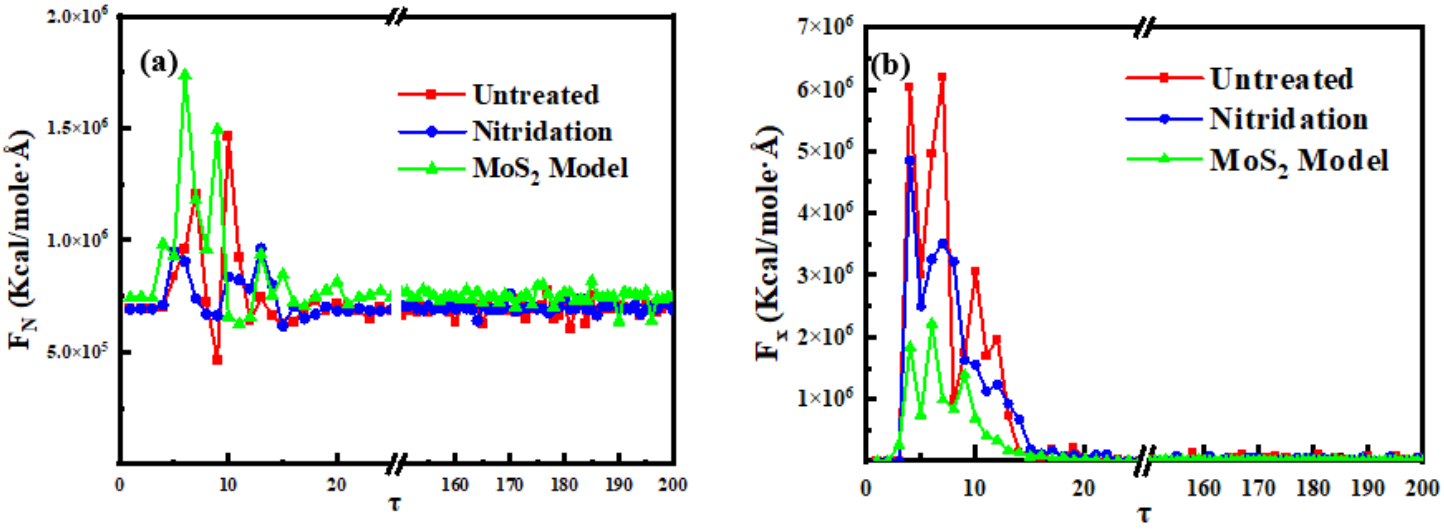

Figure 9

Changing regulation of (a) positive pressure and (b) frictional force with the three model.